Catal Lett (2009) 129:428–436
DOI 10.1007/s10562-008-9816-7

DMC Formation over $Ce_{0.5}Zr_{0.5}O_2$ Prepared by Complex-decomposition Method

Zhi-Fang Zhang · Zhao-Tie Liu · Zhong-Wen Liu · Jian Lu

Received: 10 October 2008 / Accepted: 4 December 2008 / Published online: 23 December 2008

Abstract The $Ce_{0.5}Zr_{0.5}O_2$ solid solution was prepared by a complex-decomposition method using different organic acids as complexants and cerium and zirconium nitrides as precursors, respectively. The characterization results of XRD, Raman, SEM, H_2-TPR, CO_2-TPD, N_2 adsorption at 77 K indicate that the physical properties of the solid solutions were significantly affected by the complexants used. These solid solutions can be used in dimethyl carbonate (DMC) synthesis from methanol and CO_2. Results indicate that crystal structure of $Ce_{0.5}Zr_{0.5}O_2$ was the key factor in determining the catalytic activity for DMC synthesis. Moreover, the catalytic activity of the $Ce_{0.5}Zr_{0.5}O_2$ was significantly decreased when phase separation as a result of the enrichment either of Ce or Zr was occurred. The BET surface area, the redox behavior, and pore properties of the solid solution, depending on the complexants used and the calcination temperature, also played less important roles in determining the catalytic activity for the titled reaction. The optimized $Ce_{0.5}Zr_{0.5}O_2$ showed high activity for the direct synthesis of DMC from CO_2 and methanol.

Z.-F. Zhang · Z.-T. Liu · Z.-W. Liu · J. Lu
Key Laboratory of Applied Surface and Colloid Chemistry, Ministry of Education, Shaanxi Normal University, 710062 Xi'an, People's Republic of China

Z.-T. Liu (✉) · Z.-W. Liu (✉)
School of Chemistry & Materials Science, Shaanxi Normal University, 710062 Xi'an, People's Republic of China
e-mail: ztliu@snnu.edu.cn

Z.-W. Liu
e-mail: zwliu@snnu.edu.cn

Z.-F. Zhang
College of Chemistry & Chemical Industry, Yulin College, 719000 Yulin, People's Republic of China

Keywords $Ce_{0.5}Zr_{0.5}O_2$ · DMC synthesis · Complex-decomposition method · CO_2 · CH_3OH · Adipic acid

1 Introduction

As an environmentally benign chemical product, dimethyl carbonate (DMC) has many potential applications, and is achieving increasing importance in the chemical industry. DMC is a versatile reagent and solvent, which is used as a chemical intermediate, such as a non-toxic carbonylating and methylating agent [1, 2]. Moreover, because of its non-toxicity, DMC can also be used as a potential gasoline additive, which has about three times higher in oxygen content than that of methyl tert-butyl ether (MTBE) [3].

So far, several reaction routes for the synthesis of DMC have been studied [4]. Among the investigated methods, the direct synthesis of DMC from CO_2 and CH_3OH (Eq. 1) [4] is the more preferred route as it follows the viewpoint of "Sustainable Society" and "Green Chemistry" [5]. Thus, many works have been reported [6–14].

$$2CH_3OH + CO_2 \rightarrow (CH_3O)_2CO + H_2O \quad (1)$$

Among the catalysts investigated, such as organometallic compounds [6], carbonate salts [7] and oxides [7–9], the $Ce_xZr_{1-x}O_2$ solid solutions show potentially high catalytic performance [10–12]. One of the main reasons may be that these solid solutions have both the acidic and basic properties [13] that are an important factor for the selective synthesis of DMC from CH_3OH and CO_2 [10, 14].

Moreover the cerium or cerium-mixed oxides displaying high oxygen storage capacity (OSC) have been extensively investigated due to their wide applications in catalysis,

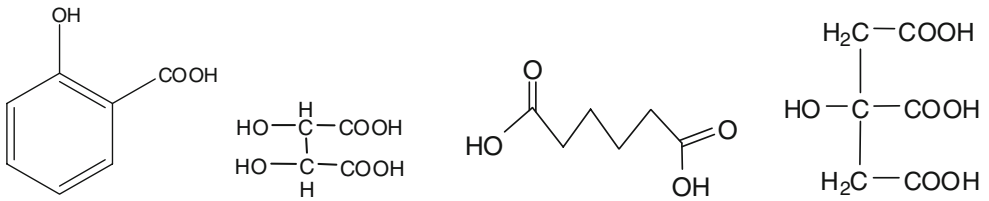

Salicylic acid Tartaric acid Adipic acid Citric acid

Scheme 1 Structures of acidic complexant used for the preparation of $Ce_{0.5}Zr_{0.5}O_2$

ultraviolet radiation absorbers, solid oxide fuel cells, and so forth [15–17]. It is commonly known that the Ce-based materials with high surface area and stability are desirable for catalytic applications. The $Ce_xZr_{1-x}O_2$ solid solutions are well known to distinctly improve the thermal stability, surface area, and reducibility of the three-way catalysts [18]. Generally, the wet chemical processes [19–23] such as complex-decomposition method, co-precipitation, and hydrothermal methods are used for the synthesis of $Ce_xZr_{1-x}O_2$ solid solutions. Among these methods, the co-precipitation method was widely used, but there were some difficulties such as the selection of the precipitators, the conditions of the titration and dehydration. Thus, it is difficult to prepare $Ce_xZr_{1-x}O_2$ solid solutions with higher surface area and OSC. In the case of complex-decomposition method, it is found that citric acid as a complexant is very attractive since it yields products with high purity, homogeneity, well-controlled properties, and it is a low temperature process as well.

In this work, we used different complex agents as shown in Scheme 1, the $Ce_{0.5}Zr_{0.5}O_2$ solid solutions with significantly varied physical and structural properties were obtained, and applied for the titled reaction. The catalytic performance of $Ce_{0.5}Zr_{0.5}O_2$ was well correlated with its physical and structural properties.

2 Experimental

2.1 Preparation of $Ce_{0.5}Zr_{0.5}O_2$

The solid solution of $Ce_{0.5}Zr_{0.5}O_2$ was prepared by complex-decomposition method using $Ce(NO_3)_3 \cdot 6H_2O$ and $Zr(NO_3)_4 \cdot 4H_2O$ as the cerium and zirconium precursors, respectively. First, 100 mL of the mixed solution of $Ce(NO_3)_3 \cdot 6H_2O$ and $Zr(NO_3)_4 \cdot 4H_2O$ in ethanol [0.3 mol L^{-1}, $Ce^{3+}/Zr^{4+} = 1.0$ (molar ratio)] was put into a 500 mL beaker. Then, the solution of acid (salicylic acid, tartaric acid, adipic acid, or citric acid) in ethanol (0.3 mol L^{-1}, 100 mL) was slowly added into the mixed solution of $Ce(NO_3)_3$ and $Zr(CO_3)_4$ under stirring. The mixture was further stirred for 24 h at a room temperature, and a sol was obtained after vaporizing the solvent at 353 K. After drying in air at 353 K for 24 h, the sol was changed into a xerogel. Finally, solid solution was obtained by calcining the xerogel in air at 773 or 1,273 K for 4 h. The heating procedure was kept at 1 K min^{-1} from a room temperature to 373 K, holding at 373 K for 60 min, then at 3 K min^{-1} from 373 to 773 K, 5 K min^{-1} from 773 to 1,273 K, and kept at 773 or 1,273 K for 4 h. In the following, the solid solutions of $Ce_{0.5}Zr_{0.5}O_2$ calcined at 773 K prepared by using salicylic acid, tartaric acid, adipic acid, and citric acid as a complex agent were designated as S, T, A and C, and the samples calcined at 1,273 were designated as S-1273, T-1273, A-1273 and C-1273, respectively.

2.2 Catalyst Characterization

X-ray diffraction (XRD) studies were carried out on a D/Max 2550VB+/PC with Cu $K\alpha$ radiation ($\lambda =$ 1.5406 Å) and Ni filter. The X-ray tube was operated under 30 kV and 40 mA. Samples were scanned from 2θ of 20 to 80° with a step size of 0.02° and a counting time of 2.5 s per step. The morphologies were studied by SEM analyses on a Quanta 200 apparatus, Philips-FEI Co (30 kV high vacuum modes, resolution: 3.5 nm).

Textural properties were determined by N_2 adsorption-desorption at 77 K using automatic Micromeritics ASAP 2020M equipment. Data were retrieved according to the BET and BJH methods from desorption branch. The solid solutions were first degassed at 623 K for at least 6 h to remove the adsorbed impurities before isotherms were recorded.

CO_2 pulse chemisorption was performed on a Micromeritics AutoChem II 2920 instrument equipped with a thermal conductivity detector (TCD). Prior to adsorption experiments, the samples (100 mg) were pre-treated in a quartz U-tube in a helium stream at 773 K. After cooling down to a room temperature in He with a flow rate of 30 cm^3 min^{-1}, pulses of the probe molecule started. The amount of gases desorbed was determined by time integration of the TPD-curves.

The reduction behaviors of the samples were examined by temperature programmed reduction (TPR) on a Micromeritics AutoChem II 2920 instrument. 5% H_2 in argon with a flow rate of 50 cm^3 min^{-1} was used for all the experiments. The temperature was programmed from a room temperature to 1,073 K with a heating rate of 10 °C min^{-1}. The water produced by reduction was trapped into a cold trap. The consumption of H_2 was quantitatively measured by time integration of the TPR-profiles.

2.3 Catalytic Activity Test

The direct synthesis of DMC from CO_2 and CH_3OH was carried out in a stainless-steel autoclave reactor with an inner volume of 100 mL. 8 g CH_3OH (A. R., Xi'an Chemical Industries) and 0.5 g of catalyst were put into the autoclave, then the reactor was purged with carbon dioxide. After pressurizing the autoclave to a certain pressure with CO_2, the reactor was heated and magnetically stirred constantly. The reaction was carried out at different temperatures (353, 373, 393, 413, 433, and 453 K) and 20 MPa.

Products in liquid and gas phases were analyzed by a gas chromatograph (GC, SP6800, Shandong Lu'nan Co.) equipped with FID and TCD detectors. A capillary column of HP-5 was used for separating the liquid products and the unconverted CH_3OH, and a packed column of GDX-102 for separating the gaseous products.

3 Results and Discussion

3.1 XRD and Raman Characterization

It is well established that the $Ce_{1-x}Zr_xO_2$ solid solutions have three stable phases [monoclinic (*m*), tetragonal (*t*), and cubic (*c*)], and two metastable phases (*t*′, *t*″) under different conditions [13, 14, 24, 25]. However, it is difficult to determine the phases of nanocrystal $Ce_{1-x}Zr_xO_2$ based only on the XRD data [26, 27]. As reported in a recent paper [28], the *t*-phase and *c*-phase $Ce_{1-x}Zr_xO_2$ can be well differentiated by combining the XRD and Raman spectroscopy as that there are six Raman bands for *t*-ZrO_2, and only one Raman band for *c*-CeO_2.

From the XRD patterns shown in Fig. 1a, it is evident that no diffractions to either CeO_2 or ZrO_2 were observed, indicating that the $Ce_{0.5}Zr_{0.5}O_2$ solid solution was formed via the homogeneous mixing of Ce and Zr ions. Based on the diffraction at 2θ of 29.20°, the crystal size of $Ce_{0.5}Zr_{0.5}O_2$ was calculated by using Scherer formula. Irrespective of the complex agents, the crystal sizes for all the samples calcined at 773 K were quite similar (about 2.6 nm), indicating a nanocrystalline nature of the calcined powders.

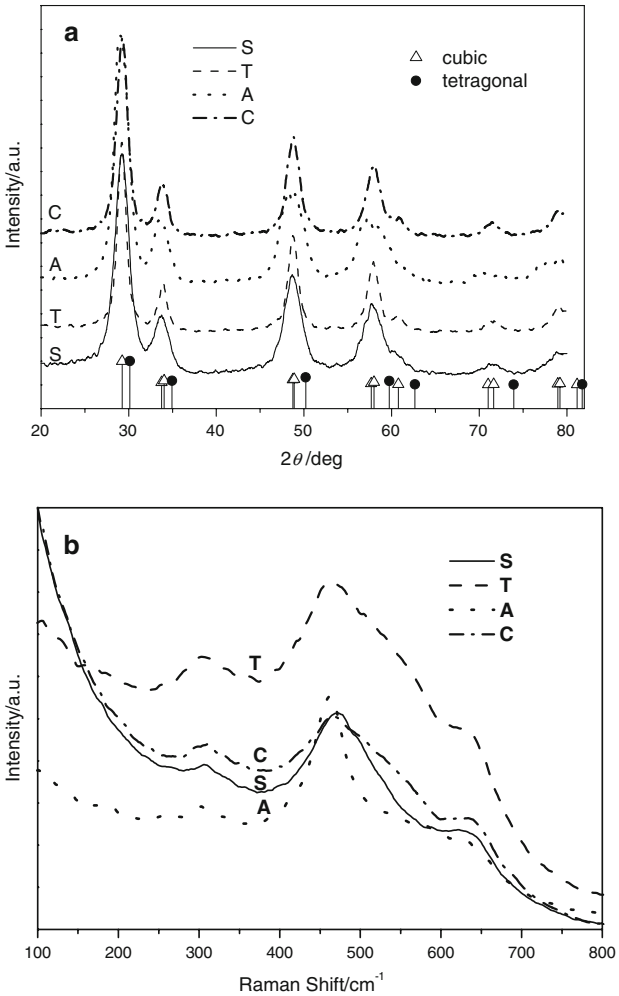

Fig. 1 The wide-angle XRD patterns (**a**) and Raman shift (**b**) of the $Ce_{0.5}Zr_{0.5}O_2$ calcined at 773 K

The Raman spectroscopy for different samples is shown in Fig. 1b. As it can be seen from Fig. 1b, the Raman-active bands at 305, 463 and 636 cm^{-1} were clearly observed for all the samples calcined at 773 K. Irrespective of the complexants, the XRD and Raman results indicated that all the samples calcined at 773 K were attributed mainly to the cubic phase $Ce_{0.5}Zr_{0.5}O_2$, indicating a less important role of complex agents in determining the crystal structure of $Ce_{0.5}Zr_{0.5}O_2$ under these conditions.

By increasing the calcination temperature to 1,273 K, some different structures were observed as given in Fig. 2. In the case of C-1273 and S-1273, a shoulder peak at 2θ of about 28.8° assigned to cubic $Ce_{0.75}Zr_{0.25}O_2$ was observable although the main phase was tetragonal $Ce_{0.5}Zr_{0.5}O_2$. However, mixtures of cubic $Ce_{0.75}Zr_{0.25}O_2$ and tetragonal ZrO_2 were dominated for the samples of T-1273 and A-1273, indicating that phase separation was significantly

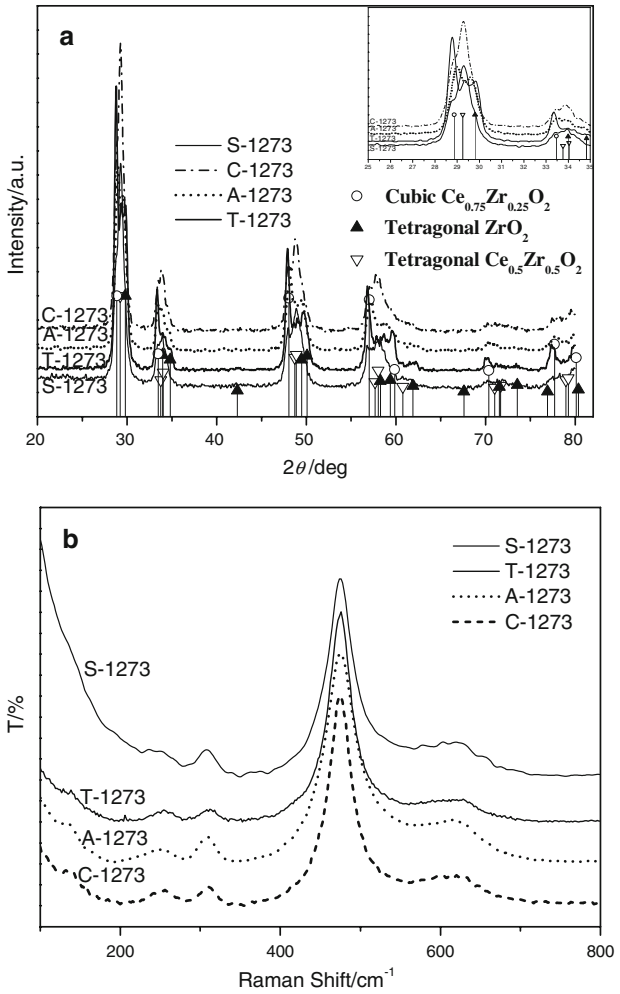

Fig. 2 The wide-angle XRD patterns (**a**) and Raman shift (**b**) of the $Ce_{0.5}Zr_{0.5}O_2$ calcined at 1,273 K

occurred, i.e., significant enrichment of Ce and Zr in $Ce_{0.5}Zr_{0.5}O_2$, during the high-temperature calcination (Fig. 2a). As a result of the phase separation, the crystal size based on XRD diffractions cannot be calculated. These results indicate that the complexant used is important to the phase separation of $Ce_{0.5}Zr_{0.5}O_2$ solid solution when the calcination temperature was at 1,273 K. Again, the complexant played a less important role in determining the phase at a higher calcination temperature of 1,273 K.

3.2 Morphology and Physical Properties

The porous properties of the samples were characterized by SEM (Figs. 3, 4) and low-temperature nitrogen adsorption (Fig. 5). The pore size distributions were determined by BJH method from the desorption branch of the N_2 adsorption-desorption isotherm at 77 K shown in Fig. 5.

From Fig. 3, the morphology of $Ce_{0.5}Zr_{0.5}O_2$ calcined at 773 K was different depending on the complex agents used. For sample S, a clear layered structure with irregular layer spaces was observed. However, the sample T showed the slit-shaped holes. Similar to sample T, sample A was composed mainly of the partly ordered slit-shaped holes. It is interesting that well distributed round pores with average pore size of about 400 nm were appeared for sample C.

From Fig. 4, the morphology of the $Ce_{0.5}Zr_{0.5}O_2$ calcined at 1,273 K was still significantly influenced by the complexant used. Moreover, irrespective of the calcination temperatures, $Ce_{0.5}Zr_{0.5}O_2$ prepared by using the same complexant showed quite similar morphologies (Figs. 3, 4). However, a clear significant sintering of the oxides calcined at 1,273 K was observable. Taking the $Ce_{0.5}Zr_{0.5}O_2$ prepared by using salicylic acid as an example, the distance between the $Ce_{0.5}Zr_{0.5}O_2$ layers for S-1273 was much shorter than that for S.

From these morphologic observations, the complex acids were speculated to act as a structure-directing agent or template via complexing with metal ions. Taking sample S as an example, all the atoms or ions of the complexant are in one plane, as shown in Scheme 2. In this case, after calcination at 773 K, the complex agent was substituted by O atoms, leading to the layered structure of the oxide. By increasing the calcination temperature to 1,273 K, the layer distance was significantly decreased as a result of the sintering effect.

As shown in Fig. 5, a type IV isotherm characterizing the mesoporous materials was observed for all the samples [29]. The hysteresis loops for sample C can be ascribed to the mixture of type H2 and H4 loops, according to the IUPAC interpretation, which are often associated with ink-bottle pores. These ink-bottle pores are expected to occur from aggregation of globular or particulate gel structure [30]. The hysteresis loops for samples T and A were close to the mixture of type H2 and H3 loops, which is often associated with heterogeneous pore networks. As there was no plateau at high P/P_o for the isotherm of S sample, it could be assigned to the type H3 loops, characterizing the adsorption of montmorillonite clay. These adsorption results are well agreeable with the SEM observations shown in Fig. 3. The calculated pore properties based on nitrogen sorption isotherm are given in Table 1. The sample A showed a remarkably higher BET surface area and total pore volume than the other samples. Moreover, the BET surface area was decreased obviously in the order of sample A, T, S and C.

The isotherms of the $Ce_{0.5}Zr_{0.5}O_2$ calcined at 1,273 K are provided in Fig. 6. Again, all the samples showed a type IV isotherm, which is the same as that of the samples calcined at 773 K. However, the adsorption capacity for the $Ce_{0.5}Zr_{0.5}O_2$ calcined at 1,273 K was much lower than that for the samples calcined at 773 K. When the hysteresis loops were considered, it is interesting that all the

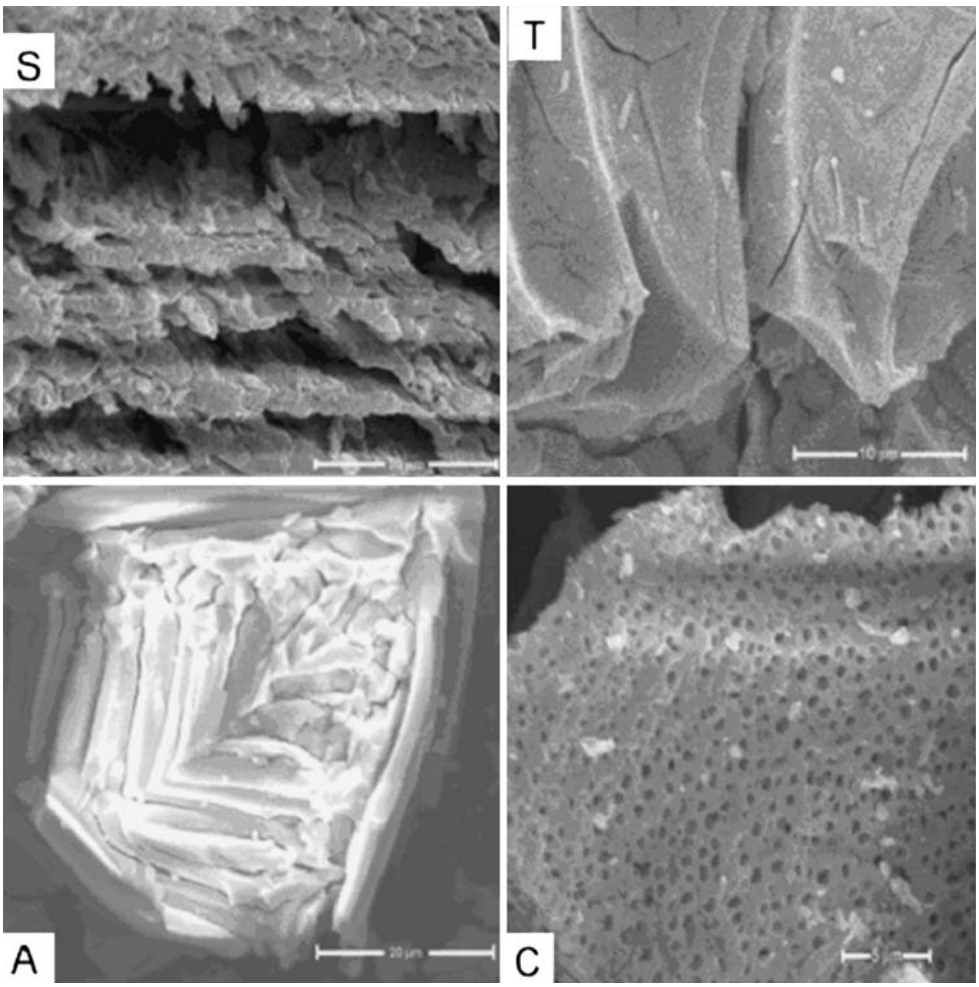

Fig. 3 The SEM micrographs of $Ce_{0.5}Zr_{0.5}O_2$ calcined at 773 K

$Ce_{0.5}Zr_{0.5}O_2$ calcined at 1,273 K displayed the same H3-type loops. From the BET surface area and pore volumes shown in Table 1, the very low surface area and pore volume for C-1273, T-1273, and A-1273 clearly indicated a significant sintering of the $Ce_{0.5}Zr_{0.5}O_2$ particles, which is agreeable with the SEM observations. In the case of S-1273, the pore volume was increased although its surface area was obviously decreased in comparison with sample S. One thing should be noted is that the average pore diameter of the $Ce_{0.5}Zr_{0.5}O_2$ calcined at 1,273 K was clearly increased in comparison with the corresponding sample calcined at 773 K. These results indicated the complex nature of the pores for the $Ce_{0.5}Zr_{0.5}O_2$ prepared by using different complexants and calcination temperatures. This will be further discussed together with the reaction results in a later section.

3.3 H_2-TPR and CO_2 Adsorption

The H_2-TPR profiles for $Ce_{0.5}Zr_{0.5}O_2$ calcined at 773 K are comparatively shown in Fig. 7. It is clear that there was only one peak for samples S, T, A, but there were two peaks observed for sample C. The peak at lower temperature of about 813 K could be ascribed to the surface reduction. The peak at higher temperature of 914 K was the reduction of the material in the bulk [8, 18, 31–34]. These results indicated that TPR patters in the lower temperature region were basically the same for the samples S, T, A, and C, irrespective of the complexants used. In the case of sample C, we speculated that the appearance of higher temperature peak was a result of the structure and porous framework of the material. As shown in Figs. 1, 3, and 5, the structure of all the $Ce_{0.5}Zr_{0.5}O_2$ calcined at 773 K was mainly dominated by the cubic phase, but only sample C was composed of ink-bottle-like pores and the others were narrow slit-like pores. This may suggest that the cubic phase with ink-bottle-like pores had both surface and bulk reducible oxygen.

After calcining the solid solution at 1,273 K, as shown in Fig. 8, all the samples showed one reduction peak. Moreover, in comparison with the results shown in Fig. 7, the reduction profile at peak maximum was shifted towards

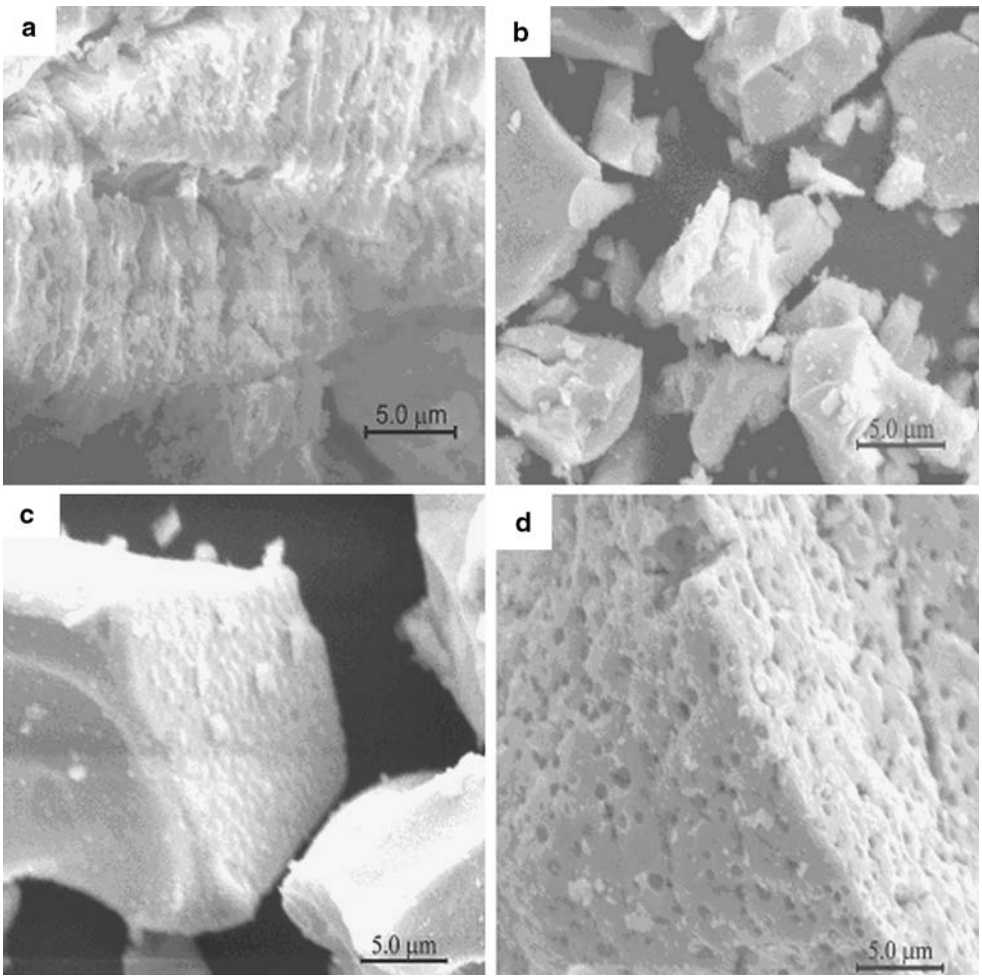

Fig. 4 The SEM micrographs of S-1273 (**a**), T-1273 (**b**), A-1273 (**c**), and C-1273 (**d**)

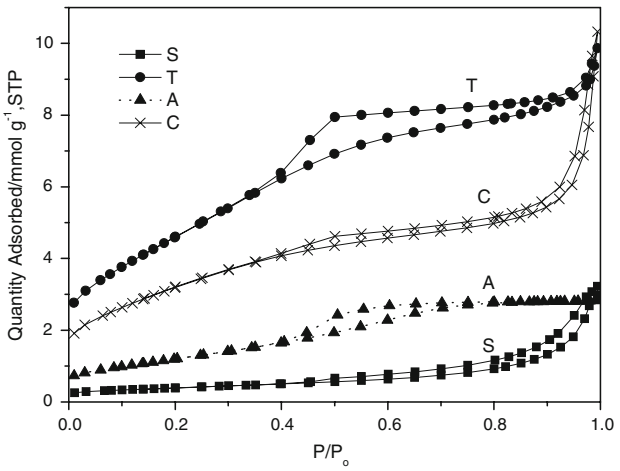

Fig. 5 Nitrogen adsorption isotherms for the $Ce_{0.5}Zr_{0.5}O_2$ calcined at 773 K

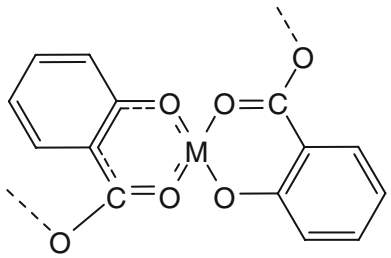

Scheme 2 The proposed structure of complex for salicylic acid

higher temperature, respectively. It was noticeable that the peak reduction temperature for S-1273 was about 842 K, which is significantly lower than those for the other three samples (above 900 K). Moreover, the T-1273 sample showed obviously higher peak maximum than the remaining three samples, which have similar peak maximum.

To probe the acid–base properties of the solid solutions, $Ce_{0.5}Zr_{0.5}O_2$ calcined at 773 K was studied by CO_2 adsorption. As shown in Table 1, the $Ce_{0.5}Zr_{0.5}O_2$ with the higher BET surface area showed the higher amount of CO_2 adsorbed. Moreover, the almost linear increase of the amount of CO_2 adsorbed with the increase of the BET

Table 1 Structural properties of $Ce_{0.5}Zr_{0.5}O_2$ and its catalytic activity for the production of DMC

Samples	BET surface area ($m^2\ g^{-1}$)	Pore volume ($cm^3\ g^{-1}$)	Average pore width (nm)	Pore center (nm)	CO_2 absorption ($cm^3\ g^{-1}$, STP)	DMC[a] (mmol)
S	52.54	0.11	14.2	3.7	1.50	0.16
T	63.81	0.38	3.9	3.6	2.10	0.20
A	166.80	1.05	3.9	3.7	6.19	0.33
C	43.35	0.35	5.5	3.2	1.15	0.11
S-1273	10.87	0.56	22.0	2.4, 45.0	–	1.75
T-1273	1.65	0.01	19.6	3.5, 10.0	–	0.00
A-1273	2.50	0.01	29.7	10.0, 10.4	–	0.33
C-1273	2.13	0.01	25.0	3.3, 10.0	–	0.34

[a] The amount of DMC formed under the conditions of $T = 373$ K, $t = 24$ h, $CH_3OH = 8.0$ g, and 0.5 g catalyst

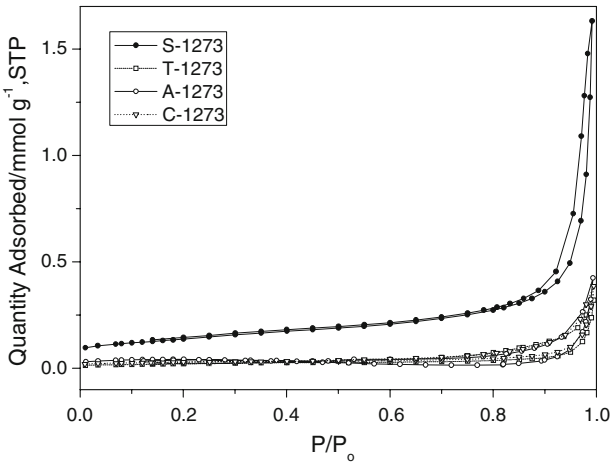

Fig. 6 Nitrogen sorption isotherms for the $Ce_{0.5}Zr_{0.5}O_2$ calcined at 1,273 K

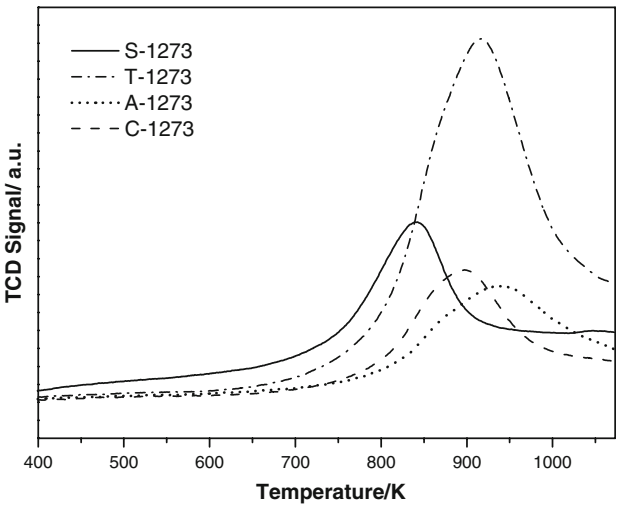

Fig. 8 H_2-TPR profiles for the $Ce_{0.5}Zr_{0.5}O_2$ calcined at 1,273 K

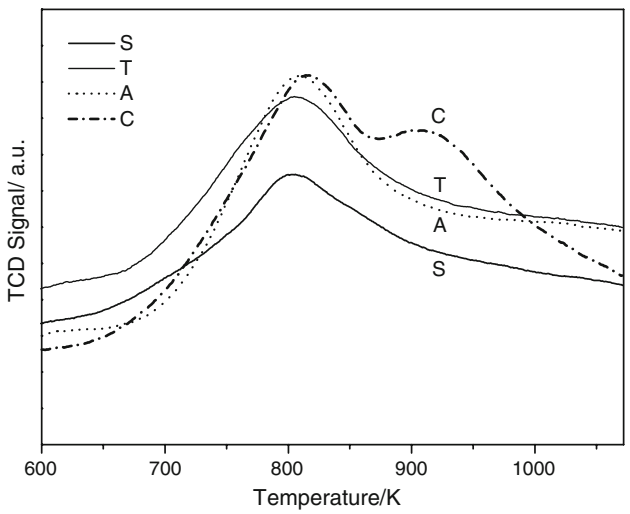

Fig. 7 H_2-TPR profiles for the $Ce_{0.5}Zr_{0.5}O_2$ calcined at 773 K

surface area of $Ce_{0.5}Zr_{0.5}O_2$ suggested the uniform surface acid–base properties of the solid solutions. This also confirmed the formation of the $Ce_{0.5}Zr_{0.5}O_2$ solid solutions, i. e., the homogeneously mixed Ce and Zr ions.

3.4 Catalytic Activity for DMC Synthesis

As shown in Table 1, under the same reaction conditions, the amount of DMC formed was significantly changed with the solid solutions of $Ce_{0.5}Zr_{0.5}O_2$. Over the $Ce_{0.5}Zr_{0.5}O_2$ calcined at 773 K, there were three-times differences for the amount of DMC formed, i.e., the sample A produced the highest amount of DMC of 0.33 mmol and the sample C of 0.11 mmol. When the $Ce_{0.5}Zr_{0.5}O_2$ calcined at 1,273 K was applied for the titled reaction, the most important observation was that S-1273 produced very high amount of DMC (1.75 mmol) while there was no

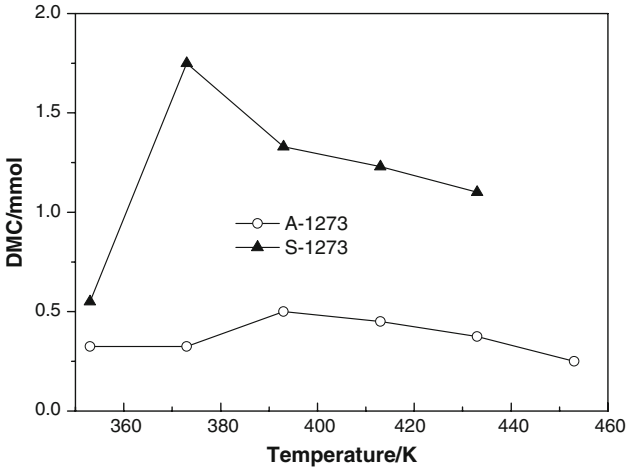

Fig. 9 Effect of reaction temperature on DMC synthesis over $Ce_{0.5}Zr_{0.5}O_2$ (reaction conditions: $p = 20$ MPa, $t = 24$ h, $CH_3OH = 8.0$ g, and 0.5 g catalyst)

detectable DMC formed over T-1273. In the case of A-1273 and C-1273, the amount of DMC formed was almost the same, which is also close to the value over sample A.

As the S-1273 showed much higher activity towards DMC synthesis, the effect of reaction temperature was investigated, and the results are given in Fig. 9. For a comparison purpose, the A-1273 was also studied at different temperatures. From Fig. 9, it is clear that there was a maximum value for the amount DMC formed with the increase of reaction temperature from 353 to 453 K. Taking the temperature effect on kinetics and thermodynamics of DMC synthesis into account, this is expectable, and well understandable. Irrespective of the reaction temperatures, S-1273 showed much higher catalytic activity for DMC synthesis than A-1273.

4 Discussion

The varied catalytic activity of $Ce_{0.5}Zr_{0.5}O_2$ must be closely related to its structural properties. XRD and Raman results indicated that solid solutions of the cubic $Ce_{0.5}Zr_{0.5}O_2$ were formed for all the samples calcined at 773 K. However, phase separation was occurred for the samples calcined at 1,273 K, especially for T-1273 and A-1273. Moreover *t*-phase $Ce_{0.5}Zr_{0.5}O_2$ was dominated for sample S-1273 and C-1273 while mixtures of cubic $Ce_{0.75}Zr_{0.25}O_2$ and tetragonal ZrO_2 were prevailed for the samples of T-1273 and A-1273. Combining these crystal structure data and the reaction results, it is reasonable to propose that *t*-phase solid solution of $Ce_{0.5}Zr_{0.5}O_2$ is more active for DMC synthesis than *c*-phase $Ce_{0.5}Zr_{0.5}O_2$. Moreover, by combing the reaction and characterization results of S-1273, T-1273, and C-1273, it is rational that phase separation of $Ce_{0.5}Zr_{0.5}O_2$ deteriorated the catalytic activity towards DMC synthesis.

The different catalytic activity of S-1273 and C-1273, which have similar crystal structure, phase composition, average pore width, may be explained as the big difference in BET surface area and pore volume. The S-1273 with a higher BET surface area and pore volume can provide more active sites for catalyzing DMC synthesis, leading to higher amount of DMC formed. Alternatively, combining the results in Table 1 and Fig. 8, the much higher catalytic activity of S-1273 for DMC synthesis may also be explained as the much lower redox temperature of the solid solution.

By examining the amount of DMC formed and the BET surface area of samples S, T, A, and C, the amount of DMC was increased almost linearly with the increase of BET surface area, and there were no simple relationships with either pore volume or average pore diameter. Thus, for $Ce_{0.5}Zr_{0.5}O_2$ having the same crystal structure, BET surface area was also importance in determining the activity for DMC synthesis. Moreover, comparing the data for $Ce_{0.5}Zr_{0.5}O_2$ calcined at 773 K (Table 1), there was no strong and clear dependence between the capacity of CO_2 adsorption and the activity of DMC synthesis. Thus, BET surface area and the easiness of the reducible oxygen are more important factors than the acid–base property of the solid solution in determining the catalytic activity.

We should note that the mass transfer can be facilitated over $Ce_{0.5}Zr_{0.5}O_2$ with a larger pore diameter and pore volume, leading to a higher catalytic activity, as reflected from the data in Table 1.

Based on the above results and reasoning, it is expected a homogeneous *t*-phase $Ce_{0.5}Zr_{0.5}O_2$ with higher surface area and pore volume, suitable pore diameter, and higher capacity of easily reducible oxygen is a desirable catalyst for DMC synthesis.

5 Conclusions

The $Ce_{0.5}Zr_{0.5}O_2$ solid solutions with different morphologies and crystal structures were prepared by complex-decomposition method using salicylic acid, tartaric, citric acid and adipic acid as a complexant, respectively. The very high surface area of $Ce_{0.5}Zr_{0.5}O_2$ (about 170 $m^2\ g^{-1}$) was obtained by using adipic acid as a complexant.

Irrespective of the complexants used, XRD results revealed that a homogeneous solid solution was formed for the $Ce_{0.5}Zr_{0.5}O_2$ calcined at 773 K. However, mixed phases of $Ce_xZr_{1-x}O_2$ were formed as a result of the enrichment either of Ce or Zr when it was calcined at

1,273 K. Furthermore, the enrichment either of Ce or Zr in $Ce_{0.5}Zr_{0.5}O_2$ was strongly dependent on the complexants used. Characterization results indicate that the calcination temperature was much important in determining the crystal structure of $Ce_{0.5}Zr_{0.5}O_2$. The morphology, BET surface area, and redox ability of the prepared $Ce_{0.5}Zr_{0.5}O_2$ were clearly changed with the complexant used, and was tentatively explained.

The prepared $Ce_{0.5}Zr_{0.5}O_2$ showed a good catalytic activity for the selective DMC synthesis from CH_3OH and CO_2. A clear relationship between the amount of DMC formed and the crystal structure, BET surface area, pore properties, and the redox behavior of the $Ce_{0.5}Zr_{0.5}O_2$ calcined at different temperatures was observed. The crystal structure of the $Ce_{0.5}Zr_{0.5}O_2$ was proposed to be a key factor in determining the catalytic activity. Moreover, the catalytic activity of the $Ce_{0.5}Zr_{0.5}O_2$ was significantly decreased when phase separation of the solid solution was occurred. The BET surface area, pore properties, and the redox properties of the $Ce_{0.5}Zr_{0.5}O_2$ also played a less important role in determining its catalytic activity. The catalytic reaction results were well explained based on these factors.

Acknowledgments The authors gratefully acknowledge the financial support from the Specialized Research Fund for the Doctoral Program of Higher Education (Grant No. 20070718003). We are also full of gratitude for the support provided by Natural Science Foundation of Shaanxi Province (2007B07).

References

1. Selva M, Marquez CA, Tundo P (1994) J Chem Soc Perkin Trans 1:1323
2. Bomben A, Marques CA, Selva M, Tundo P (1995) Tetrahedron 51:11573
3. Pacheco MA, Marshall CL (1997) Energy Fuels 11:2
4. Zhao TS, Han YH, Sun YH (1998) Petrochem Technol (Chinese) 27:457
5. Peppel WJ (1958) Ind Eng Chem 50:767
6. Tomishige K, Sakaihori T, Ikeda Y, Fujimoto K (1999) Catal Lett 58:225
7. Tomishige K, Furusawa Y, Ikeda Y, Asadullah M, Fujimoto K (2001) Catal Lett 76:1
8. Yoshida Y, Arai Y, Kado S, Kunimori K, Tomishige K (2006) Catal Today 115:95
9. Cutrufello MG, Ferino I, Solinas V, Primavera A, Trovarelli A, Auroux A, Picciau C (1999) Phys Chem Chem Phys 1:3369
10. Choi JC, Sakakura T, Sako T (1999) J Am Chem Soc 121:3793
11. Chen XZ, Hu CW, Su JH, Yu T, Gao ZM (2006) Chin J Catal 27:485
12. Fang S, Fujimoto K (1996) Appl Catal A General 142:L1
13. Yashima M, Morimoto K, Ishizawa N, Yoshimura M (1993) J Am Ceram Soc 76:1745
14. Yashima M, Morimoto K, Ishizawa N, Yoshimura M (1993) J Am Ceram Soc 76:2865
15. He X, Antonelli D (2002) Angew Chem Int Ed 41:214
16. Thammachart M, Meeyoo V, Risksomboon T, Osuwan S (2001) Catal Today 68:53
17. Cabañas A, Darr JA, Lester E, Poliakoff M (2001) J Mater Chem 11:561
18. Kaspar J, Fornasiero P, Graziani M (1999) Catal Today 50:285
19. Dhage SR, Gaikwad SP, Muthukumar P, Ravi V (2004) Mater Lett 58:2704
20. Deptula A, Carewska M, Olczak T, Lada W, Croce F (1993) J Electrochem Soc 140:2294
21. Chick LA, Pederson LR, Maupin GD, Bates JL, Thomas LE, Exarhos GJ (1990) Mater Lett 10:6
22. Potdar HS, Deshpande SB, Khollam YB, Deshpande AS, Date SK (2003) Mater Lett 57:1066
23. Roh HS, Jun KW, Dong WS, Park SE, Baek YS (2001) Catal Lett 74:31
24. Yashima M, Arashi H, Kakihana M, Yoshimura M (1994) J Am Ceram Soc 77:1067
25. Yashima M, Ohtake K, Kakihana M, Yoshimura M (1994) J Am Ceram Soc 77:2773
26. Lo′pez EF, Escribano VS, Panizza M, Carnasciali MM, Busca G (2001) J Mater Chem 11:1891
27. McBride JR, Hass KC, Poindexter BD, Weber WH (1994) J Appl Phys 76:2435
28. Yuan Q, Liu Q, Song WG, Feng W, Pu WL, Sun LD, Zhang YW, Yan CH (2007) J Am Chem Soc 129:6698
29. Sing KSW, Everet DH, Haul RAW, Moscou L, Pierotti PA, Rouquerol J, Siemieniewska T (1985) Pure Appl Chem 57:603
30. Rouquerol J, Avnir D, Fairbridge CW, Everett DH, Haynes JH, Pernicone N, Ramsay JDF, Sing KSW, Unger KK (1994) Pure Appl Chem 66(8):1739
31. Otsuka K, Wang Y, Nakamura M (1999) Appl Catal A 183:317
32. Trovarelli A, Zamar F, Llorca J, de Leitenburg C, Dolcetti G, Kiss JT (1997) J Catal 169:490
33. Yao HC, Yu Yao YF (1984) J Catal 86:254
34. Fally F, Perrichon V, Vidal H, Kaspar J, Blanco G, Pintado JM, Bernal S, Colon G, Daturi M, Lavalley JC (2000) Catal Today 59:373